arXiv:1407.2852v1 [cond-mat.quant-gas] 10 Jul 2014

Spectral and entanglement properties of the bosonic Haldane insulator

Satoshi Ejima, Florian Lange, and Holger Fehske
Institut für Physik, Ernst-Moritz-Arndt-Universität Greifswald, 17489 Greifswald, Germany
(Dated: July 11, 2014)

We discuss the existence of a nontrivial topological phase in one-dimensional interacting systems described by the extended Bose-Hubbard model with a mean filling of one boson per site. Performing large-scale density-matrix renormalization group calculations we show that the presence of nearest-neighbor repulsion enriches the ground-state phase diagram of the paradigmatic Bose-Hubbard model by stabilizing a novel gapped insulating state, the so-called Haldane insulator, which, embedded into superfluid, Mott insulator and density wave phases, is protected by the lattice inversion symmetry. The quantum phase transitions between the different insulating phases were determined from the central charge via the von Neumann entropy. The Haldane phase reveals a characteristic four-fold degeneracy of the entanglement spectrum. We finally demonstrate that the intensity maximum of the dynamical charge structure factor, accessible by Bragg spectroscopy, features the gapped dispersion known from the spin-1 Heisenberg chain.

PACS numbers: 05.30.Jp, 75.10.Pq, 64.70.Tg, 03.67.-a

A quarter-century after Haldane's conjecture of an appearance of finite gap in the integer-spin chain [1], the so-called Haldane phase protected by the lattice inversion symmetry attracts renewed attention from a topological point of view. Such a topological protected state, characterized by symmetries and a finite bulk gap, is termed now as a symmetry-protected topological (SPT) ordered phase [2, 3]. In higher dimensions, the so-called Kane-Mele topological band insulator of noninteracting fermions [4, 5] exhibits a SPT state protected by $U(1)$ and time-reversal symmetries. Since particles in real materials normally interact, it is not sufficient to study SPT order for non-interacting systems. To analyze SPT states in interacting systems two main approaches have been proposed. The first is based on the definition of appropriate topological invariants within a Green function scheme [6]. It has been successfully applied to the one-dimensional (1D) Peierls–Hubbard model [7, 8]. The second uses the entanglement spectrum as a fingerprint of topological order [9]. Here the lowest entanglement level reflects the degree of degeneracy corresponding to symmetries and the edge states of the system. This has been worked out for various spin chains [3, 10, 11].

Interestingly a hidden SPT phase was also found in interacting boson systems with long-range repulsion [12]. This phase resembles the Haldane gapped phase of the quantum spin-1 Heisenberg chain. Indeed, assuming that the site occupation of an 1D extended Bose-Hubbard model (EBHM) with nearest-neighbor interaction is restricted to $n_j = 0, 1$ or 2, the system can be described by an effective spin-1 model with $S^z_j = n_j - \rho$ for a mean boson filling factor $\rho = 1$. The Haldane insulator (HI) then appears between the conventional Mott insulator (MI) and the density wave (DW) phases at intermediate couplings [12, 13]. Field theory predicts the MI-HI transition to be in the Luttinger liquid universality class with central charge $c = 1$, whereas the HI-DW transition belongs to the Ising universality class with $c = 1/2$ [13]. Very recent quantum Monte Carlo simulations [14] reveal in addition a supersolid phase competing with the HI.

In this work, we focus on the characterization of the EBHM's ground-state and spectral properties from an entanglement point of view. Using the (dynamical) density-matrix renormalization group (DMRG) technique [15, 16], we show that the lowest entanglement level in the nontrivial topological HI phase is four-fold degenerate. The universality classes of the MI-HI and HI-DW transitions are determined from the central charge in accordance with what is obtained from field theory. Most notably we demonstrate that the dynamical charge structure factor can be used to unambiguously discriminate the HI from the MI and DW phases.

The Hamiltonian of the EBHM is defined as

$$\hat{\mathcal{H}} = -t\sum_j (\hat{b}^\dagger_j \hat{b}_{j+1} + \hat{b}_j \hat{b}^\dagger_{j+1}) + U\sum_j \hat{n}_j(\hat{n}_j - 1)/2 + V\sum_j \hat{n}_j \hat{n}_{j+1}, \tag{1}$$

where $\hat{b}^\dagger_j$, $\hat{b}_j$, and $\hat{n}_j = \hat{b}^\dagger_j \hat{b}_j$ are, respectively, the boson creation, annihilation, and number operators at the lattice site j. The nearest-neighbor boson transfer amplitude is given by t; U and V parametrize the Coulomb repulsions between bosons resting at the same and neighboring sites. While t causes the bosons to delocalize, promoting a superfluid (SF) phase at weak interactions, U (V) tends to stabilize a MI (DW) when the interaction dominates over the kinetic energy scale set by t.

In the framework of the DMRG the entanglement properties of the EBHM can be analyzed as follows. Consider the reduced density matrix $\rho_\ell = \mathrm{Tr}_{L-\ell}[\rho]$ of a block of length ℓ out of a periodic system of size L. Then the bipartite entanglement spectrum $\{\xi_\alpha\}$ is defined as those of a fictitious Hamiltonian $\bar{\mathcal{H}}$ defined via $\rho_\ell = e^{-\bar{\mathcal{H}}}$. As a consequence the ξ_α can be extracted from the weights λ_α of the reduced density matrix ρ_ℓ by

$\xi_\alpha = -2\ln\lambda_\alpha$. Adding up, along the calculations, the λ_α, we have direct access to the von Neumann entropy, $S_L(\ell) = -\mathrm{Tr}_\ell[\rho_\ell \ln \rho_\ell]$. On the other hand, from conformal field theory [17] one has $S_L(\ell) = \frac{c}{3}\ln\left[\frac{L}{\pi}\sin\left(\frac{\pi\ell}{L}\right)\right] + s_1$ with the non-universal constant s_1. Thus we can easily determine the central charge c by DMRG. Since the most precise data for $S_L(\ell)$ were obtained when the length ℓ of the subblock equals half the system size L, the central charge should be determined from the relation [18]

$$c^*(L) = \frac{3[S_L(L/2-1) - S_L(L/2)]}{\ln[\cos(\pi/L)]}\,, \qquad (2)$$

rather than directly using the above expression for $S_L(\ell)$.

In contrast to hitherto existing open boundary DMRG studies of the EBHM [12, 13, 19] we use periodic boundary conditions (PBCs). As shown for the regular Bose-Hubbard model this is advantageous calculating the central charge [20, 21]. Beyond that we benefit from the fact that no artificial on-site potentials at the edges will affect our results. To reach the same system sizes as with open boundary conditions (OBCs), we limit the number of bosons per site. Throughout this work we use $n_b = 2$; here the EBHM corresponds to an effective spin-1 Heisenberg model. We have convinced ourselves that at sufficiently large U the boson truncation does not alter qualitatively the results presented in the following (solely, in the weak coupling regime, the extension of the SF phase is somewhat underestimated). Let us finally note that we keep up to $m = 2400$ states in the DMRG runs, so that the discarded weight is typically smaller than 1×10^{-8}. For the dynamical DMRG calculations we take $m = 800$ states to compute the ground state during the first five DMRG sweeps, and afterwards use 400 states evaluating the dynamical properties.

As stated above the ground-state phase diagram of the EBHM (1) with $n_b = 2$ exhibits three differing insulator phases, as well as a superfluid state at weak interactions U/t, V/t. The stability regions of the various phases are pinpointed by Fig. 1. Let us emphasize that in the intermediate-coupling region ($3 \lesssim U \lesssim 8$), the central charge is best suited for detecting the MI-HI (HI-DW) quantum phase transition since the system becomes critical at the transition points with $c = 1$ (1/2).

Figure 2 (a) illustrates the behavior of the central charge c^* obtained numerically as a function of V/t at fixed $U/t = 5$. With increasing system size L two sharp peaks develop, indicating the MI-HI and HI-DW transition points. For $L = 128$, we found $c^* \simeq 0.999$ in the former case and $c^* \simeq 0.494$ in the latter case, i.e., the numerical error, $|c^*(L) - c|/c$, is about 1% if compared with the field theoretical predictions. Since the positions of the peaks only weakly depend on the system size, the transition points can be determined by extrapolating the values of the critical $V(L)$ to the thermodynamic limit $L \to \infty$. MI-HI transition points are also extracted from the level spectroscopy of two lowest-lying energies with anti-periodic boundary conditions (APBCs), $\hat{b}^{(\dagger)}_{L+1} \to -\hat{b}^{(\dagger)}_1$. This equates to the twisted boundary methods [22] with the spin operators $\hat{S}^x_{L+1} \to -\hat{S}^x_1$ and $\hat{S}^y_{L+1} \to -\hat{S}^y_1$ applied to the spin-1 XXZ chain [23], see also Ref. [24]. The obtained transition points can be linearly extrapolated to the thermodynamic limit as in the inset of Fig. 2(a), showing a perfect agreement with the critical points obtained in the main panel.

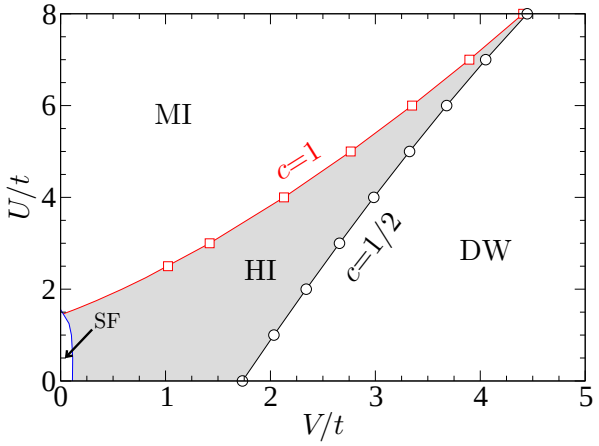

FIG. 1. (color online). DMRG phase diagram of the 1D constrained extended Bose-Hubbard model with $n_b = 2$ and $\rho = 1$. Shown are the Mott insulator (MI), Haldane insulator (HI), density wave (DW), and superfluid (SF) phases. The MI-HI (squares) and HI-DW (circles) transition points are determined via the central charge $c = 1$ and $c = 1/2$, respectively, which can be extracted from the von Neumann entropy [cf. Fig. 2 (b)]. MI-HI transition points are confirmed by a finite-size scaling of the two lowest energy levels with APBCs. Relaxing the boson constraint the SF region extends.

The excitation gaps behave differently in various insulating phases [12, 13]: While the single-particle gap $\Delta_c = E_0(N+1) + E_0(N-1) - 2E_0(N)$ is finite in all three insulator phases, except for the MI-HI transition point, the neutral gap $\Delta_n = E_1(N) - E_0(N)$ closes both at the MI-HI and HI-DW transitions [$E_0(N)$ and $E_1(N)$ denote the energies of the ground state and first excited state of the N-particle system, respectively]. This is corroborated by Fig. 2 (b). A similar behavior of the neutral gap has been observed for the SPT phases of spin-1/2 ladder systems [25]. Note that the phase boundaries obtained by our PBC DMRG calculation at intermediate and strong couplings basically agree with very recent DMRG data for OBCs [19, 26]. In the weak-coupling regime, on the other hand, our phase diagram differs from former studies due to the $n_b = 2$ restraint. Accordingly the MI-SF transition at $V = 0$ occurs at a smaller value, $U \simeq 1.555t$, if compared to the critical U/t derived from the Tomonaga-Luttinger liquid parameter [27]. The appearance of the SF phase, which can be understood as a Luttinger liquid with $c = 1$ [28], together with strong finite-size effects

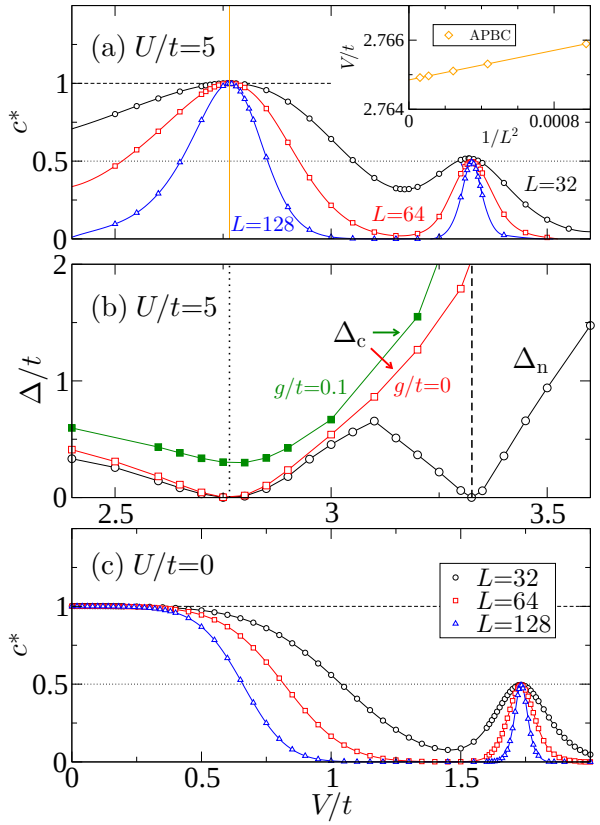

FIG. 2. (color online). Panel (a): Central charge c^* of the EBHM with $U/t = 5$, indicating the MI-HI (HI-DW) transition point with $c = 1$ ($c = 1/2$). The inset shows a finite-size scaling of the MI-HI transition points from the energy difference with APBCs. Panel (b): Extrapolated data for the charge gap Δ_c (open squares) and neutral gap Δ_n (open circles) at $U = 5t$. Vertical lines mark the transition points estimated from c^*. While Δ_n vanishes at both MI-HI and HI-DW boundaries, the charge gap Δ_c closes at the MI-HI transition only. Turning-on an inversion-symmetry breaking perturbation [$g/t = 0.1$, see Eq. (3)] Δ_c stays finite $\forall V/t$ (filled squares). Panel (c): c^* at $U = 0$. Now the SF/MI-HI transition point is hardly to detect.

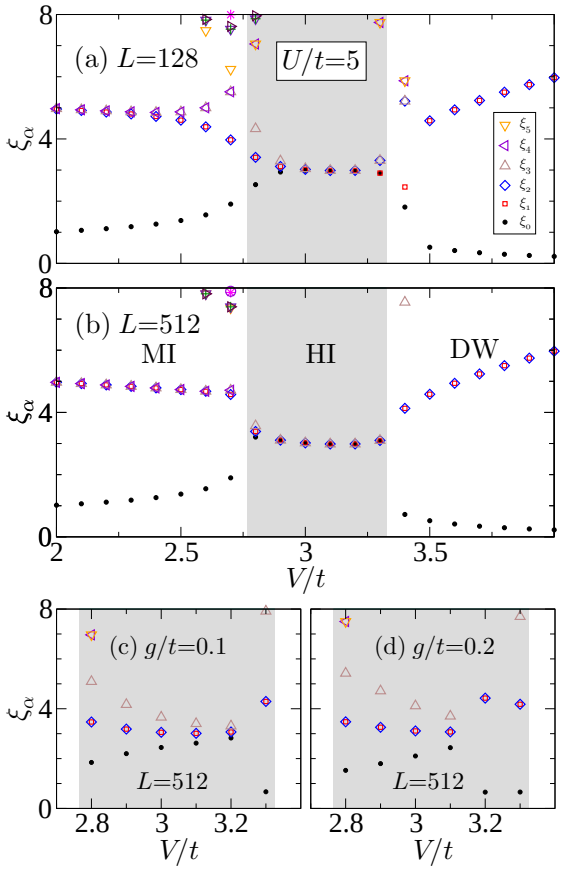

FIG. 3. (color online). Entanglement spectrum ξ_α of the EBHM with $U/t = 5$. If exciting the degeneracy of the entanglement levels becomes more perfect as the system size increases (cf. data for $L = 128$ [panel (a)] with those for 512 [panel (b)]). A perturbation (3) breaking the lattice inversion symmetry lifts the degeneracy in the HI phase. This is demonstrated by panels (c) and (d) giving ξ_α for PBCs in the primary HI regime for $g/t = 0.1$ and 0.2, respectively.

prevents using c^* for detecting the MI-HI transition in this regime. Otherwise, as shown by Fig. 2 (c), the HI-DW Ising transition can still be determined from c^*, even for $U = 0$.

On these grounds, discussing the entanglement properties of the SPT state, we consider the intermediate-coupling region hereafter. Calculating the entanglement spectrum ξ_α we divide the system in halves. Then, using DMRG with PBCs, one of the block with $L/2$ sites possesses two edges (rather than a single edge in the semi-infinite chain used by the infinite-time evolving block-decimation algorithm [3]). In the HI phase the entanglement spectrum is expected to be at least four-fold degenerate, reflecting the broken $\mathbb{Z}_2 \times \mathbb{Z}_2$ symmetry. Figure 3 shows the DMRG data for ξ_α obtained at $U/t = 5$. While for $L = 128$ the four-fold degeneracy can be seen only deep inside of the HI phase, for $L = 512$ almost all HI states exhibit this degeneracy. By contrast, in the trivial MI and DW phases the lowest entanglement level is always non-degenerate. Obviously higher entanglement levels $\xi_\alpha > 8$ are also four-fold degenerate (cf. Fig. S2 of Ref. [24]).

We already stated that the HI phase is protected by the inversion symmetry of the lattice. This symmetry can explicitly be broken by adding to the Hamiltonian (1) an appropriate perturbation [13]:

$$\delta\hat{\mathcal{H}} = g \sum_j [(\hat{n}_j - \rho)\hat{b}_j^\dagger \hat{b}_{j+1} + \text{h.c.}] \,. \qquad (3)$$

As a consequence the MI-HI quantum phase transition disappears [13] and the single-particle charge gap stays finite; see the filled squares in Fig. 2 (b) displaying Δ_c for $g/t = 0.1$. One also expects that this perturbation lifts

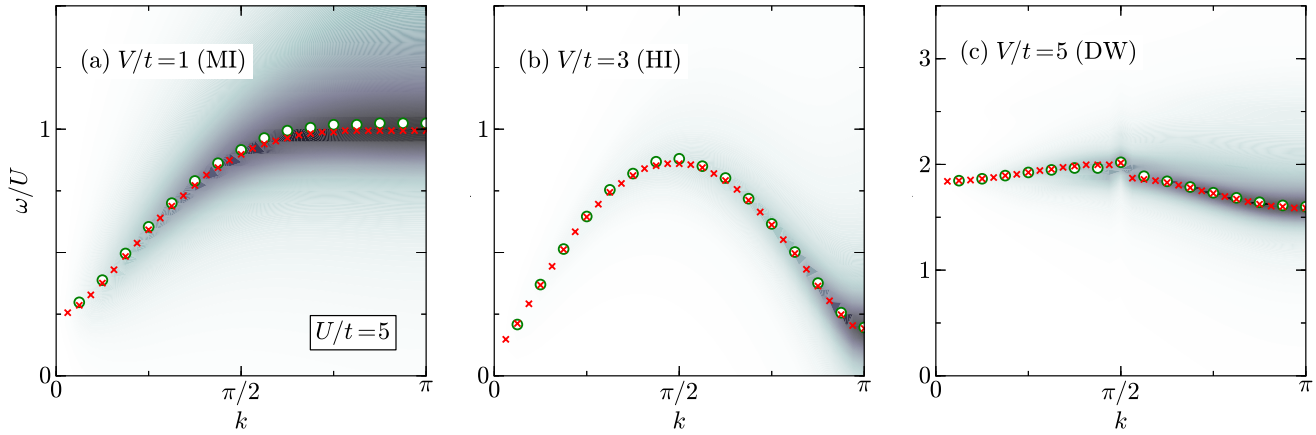

FIG. 4. (color online). Intensity plots of the dynamical structure factor $S(k,\omega)$ in the MI (a), HI (b), and DW (c) phases. Data were obtained by the dynamical DMRG technique for $L=64$ using a broadening $\eta=0.5t$. Crosses (circles) give the maximum value of $S(k,\omega)$ for $L=64$ ($L=32$ and $\eta=t$) at fixed momenta $k=2\pi j/L$ with $j=1,\cdots,L/2$.

the degeneracy of the lowest entanglement level in the HI phase. Indeed Fig. 3 (c) illustrates that any finite g dissolves the four-fold degeneracy in the HI phase, where the gap between the lowest levels increases raising g [cf. Fig. 3 (d)]. That is, the entanglement spectrum substantiates the suspicion that the lattice inversion symmetry is necessary for the nontrivial topological HI state to exist.

Since the EBHM (1) can be realized by ultracold bosonic atoms loaded in optical lattices [29] it is highly desirable to study dynamical correlation functions which are accessible by experiments. For this purpose, the kinetic-energy correlations of the effective spin-1 Heisenberg chain was proposed to be a candidate detecting the HI phase and calculated on a mean-field level of approximation [12]. Here we suggest the dynamical structure factor—which can be directly measured by momentum-resolved Bragg spectroscopy [30, 31]—to be indicative of a SPT state. This quantity is defined as

$$S(k,\omega)=\sum_n |\langle\psi_n|\hat{n}_k|\psi_0\rangle|^2\delta(\omega-\omega_n)\,, \qquad (4)$$

where $|\psi_0\rangle$ and $|\psi_n\rangle$ denote the ground state and nth excited state, respectively. The corresponding excitation energy is $\omega_n=E_n-E_0$. In the absence of the nearest-neighbor repulsion V, $S(k,\omega)$ was intensively studied by means of perturbative and dynamical DMRG techniques [20, 32]. Taking V into account, in the MI, a gap opens at $k=0$ and the spectral weight becomes concentrated in the region $k>\pi/2$, around $\omega/U\simeq 1$, just as for the standard Bose-Hubbard model. This is exemplified for $U=5t$ and $V=t$ by Fig. 4 (a). The maximum in $S(k,\omega)$ follows a cosine-dispersion which is flattened, however, near the Brillouin zone boundary for $k\geq 3\pi/4$. The situation dramatically changes when we enter the HI phase by increasing V/t, cf. Fig. 4 (b) for $V/t=3$. Now the dispersion of the maximum in $S(k,\omega)$ bends back above $k=\pi/2$, acquiring a sinus shape with (small) excitation gaps at both $k=0$ and $k=\pi$. Also the spectral weight of the dynamical charge structure factor is concentrated at $k=\pi$ and finite but very small for $\omega\ll U$. We note that the dispersion of the maximum in the HI phase is remindful of those of the spin-1 Heisenberg chain. A dispersive signal persists if we allow larger n_b (see the results presented in Ref. [24] for the EBHM with $n_b=5$). In the DW phase, the maximum of $S(k,\omega)$ is almost dispersionsless and located at $\omega\gtrsim 1.5U$ for $U/t=V/t=5$ [see Fig. 4 (c)]. The intensity is notably more confined than for the MI. Figure 4 demonstrates that the dispersion in the insulating phases barely changes if the system size is increased. In every sense, $S(k,\omega)$ behaves very differently in the MI, DW, and HI states and might therefore be used to discriminate these insulating phases.

In summary, we studied—from an entanglement point of view—the topologically nontrivial Haldane insulator, appearing in the intermediate coupling regime of the 1D Bose-Hubbard model with on-site and nearest-neighbor Coulomb interactions in the midst of Mott insulator, density-wave and superfluid phases. Using the DMRG technique, the MI-HI (HI-DW) quantum phase transition is determined with high precision from the central charge c^* that can be extracted from the von Neumann entropy. We thereby approved the universality class $c=1$ ($c=1/2$) predicted by field theory. We furthermore established a characteristic four-fold degeneracy of the lowest entanglement level in the SPT Haldane phase and demonstrated that any violation of the lattice inversion symmetry lifts this degeneracy. With the objective to stimulate further experiments on ultracold bosonic atoms in optical lattices we analyzed the dynamical charge structure factor for the extended Bose-Hubbard model and showed that this quantity can be used to distinguish the Haldane insulator, exhibiting a gapped excitation spectrum similar to the spin-1 Heisenberg-chain model, from conventional Mott and density-wave states.

Acknowledgments. The authors would like to thank S. Nishimoto and T. Yoshida for valuable discussions. This work was supported by Deutsche Forschungsgemeinschaft through SFB 652, Project B5.

[1] F. D. M. Haldane, Phys. Rev. Lett. **50**, 1153 (1983).
[2] Z.-C. Gu and X.-G. Wen, Phys. Rev. B **80**, 155131 (2009).
[3] F. Pollmann, E. Berg, A. M. Turner, and M. Oshikawa, Phys. Rev. B **85**, 075125 (2012).
[4] C. L. Kane and E. J. Mele, Phys. Rev. Lett. **95**, 146802 (2005).
[5] C. L. Kane and E. J. Mele, Phys. Rev. Lett. **95**, 226801 (2005).
[6] V. Gurarie, Phys. Rev. B **83**, 085426 (2011).
[7] S. R. Manmana, A. M. Essin, R. M. Noack, and V. Gurarie, Phys. Rev. B **86**, 205119 (2012).
[8] T. Yoshida, R. Peters, S. Fujimoto, and N. Kawakami, Phys. Rev. Lett. **112**, 196404 (2014).
[9] H. Li and F. D. M. Haldane, Phys. Rev. Lett. **101**, 010504 (2008).
[10] F. Pollmann, A. M. Turner, E. Berg, and M. Oshikawa, Phys. Rev. B **81**, 064439 (2010).
[11] Z.-X. Liu, Z.-B. Yang, Y.-J. Han, W. Yi, and X.-G. Wen, Phys. Rev. B **86**, 195122 (2012).
[12] E. G. Dalla Torre, E. Berg, and E. Altman, Phys. Rev. Lett. **97**, 260401 (2006).
[13] E. Berg, E. G. Dalla Torre, T. Giamarchi, and E. Altman, Phys. Rev. B **77**, 245119 (2008).
[14] G. G. Batrouni, R. T. Scalettar, V. G. Rousseau, and B. Grémaud, Phys. Rev. Lett. **110**, 265303 (2013).
[15] S. R. White, Phys. Rev. Lett. **69**, 2863 (1992).
[16] E. Jeckelmann, Phys. Rev. B **66**, 045114 (2002).
[17] P. Calabrese and J. Cardy, J. Stat. Mech. **(2004)** P06002.
[18] S. Nishimoto, Phys. Rev. B **84**, 195108 (2011).
[19] D. Rossini and R. Fazio, New J. Phys. **14**, 065012 (2012).
[20] S. Ejima, H. Fehske, F. Gebhard, K. zu Münster, M. Knap, E. Arrigoni, and W. von der Linden, Phys. Rev. A **85**, 053644 (2012).
[21] S. Ejima, M. J. Bhaseen, M. Hohenadler, F. H. L. Essler, H. Fehske, and B. D. Simons, Phys. Rev. Lett. **106**, 015303 (2011).
[22] A. Kitazawa, K. Nomura, and K. Okamoto, Phys. Rev. Lett. **76**, 4038 (1996).
[23] W. Chen, K. Hida, and B. C. Sanctuary, Phys. Rev. B **67**, 104401 (2003).
[24] Supplementary material.
[25] S. R. Manmana, E. M. Stoudenmire, K. R. A. Hazzard, A. M. Rey, and A. V. Gorshkov, Phys. Rev. B **87**, 081106 (2013).
[26] D. Rossini, M. Gibertini, V. Giovannetti, and R. Fazio, Phys. Rev. B **87**, 085131 (2013).
[27] S. Ejima, H. Fehske, and F. Gebhard, Europhys. Lett. **93**, 30002 (2011).
[28] T. Giamarchi, *Quantum Physics in One Dimension* (Clerendon Press, Oxford, 2003).
[29] I. Bloch, J. Dalibard, and W. Zwerger, Rev. Mod. Phys. **80**, 885 (2008).
[30] D. Clément, N. Fabbri, L. Fallani, C. Fort, and M. Inguscio, Phys. Rev. Lett. **102**, 155301 (2009).
[31] P. T. Ernst, S. Götze, J. S. Krauser, K. Pyka, D.-S. Lühmann, D. Pfannkuche, and K. Sengstock, Nature Physics **6**, 56 (2010).
[32] S. Ejima, H. Fehske, and F. Gebhard, J. Phys. Conf. Ser. **391**, 012143 (2012).

Supplementary material

Using the unbiased density matrix renormalization group (DMRG) technique with periodic boundary conditions (PBCs), in the main paper, we derived the ground-state phase diagram of the one-dimensional (1D) extended Bose-Hubbard model (EHBM), restricting the maximum number of bosons per site to be $n_b = 2$. Figure 1 showed the extent of the Haldane insulator (HI) phase, located between the conventional insulating Mott (MI) and density wave (DW) states and the superfluid (SF) phase. In the following we provide further results for the EBHM in the intermediate-coupling region, in order to guarantee that our main conclusions will be unaffected in the more general case with $n_b > 2$.

Determination of the MI-HI transition points

As stressed in the main text the 1D EBHM can be mapped onto an effective spin-1 XXZ chain model with on-site anisotropy D. Then, in the notations of Ref. [23], the three insulating MI, HI, and DW phases of the EBHM correspond to the large-D, the Haldane and the Néel phases, respectively. The Haldane phase in the spin-1 chain is described by a spin-1/2 two-leg ladder system [3, 10, 11]. As discussed in Ref. [11], with the projective representations of the symmetry group it is related to the t_0 phase of the latter system. According to Ref. [23], using Lanczos diagonalization, the large-D-Haldane phase transition points can be determined by level spectroscopy [22] of the two lowest-lying energies with twisted boundary conditions (i.e., $\hat{S}^x_{L+1} \to -\hat{S}^x_1$, $\hat{S}^y_{L+1} \to -\hat{S}^y_1$, and $\hat{S}^z_{L+1} \to \hat{S}^z_1$). Hence also the MI-HI transition points can be extracted by analyzing the two lowest-lying energies with anti-periodic boundary conditions (APBCs), i.e., $\hat{b}^{(\dagger)}_{L+1} \to -\hat{b}^{(\dagger)}_1$. As shown by

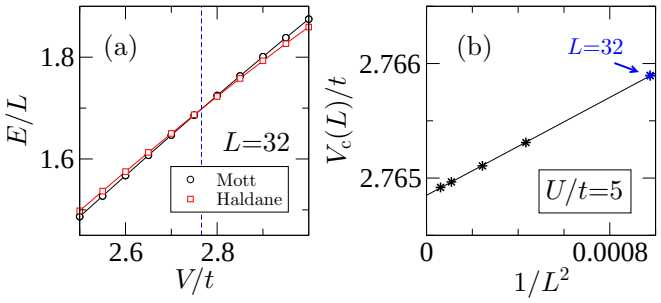

FIG. S1. (a) The V dependence of the two lowest energy eigenvalues with APBCs at $U/t = 5$ and $L = 32$. The energies of the Haldane state (squares) and the Mott insulating state (circles) cross at the MI-HI transition point. (b) The critical points $V_c(L)/t$ as extracted in the panel (a) versus inverse of the squares of the system size at $U/t = 5$ with up to $L = 128$.

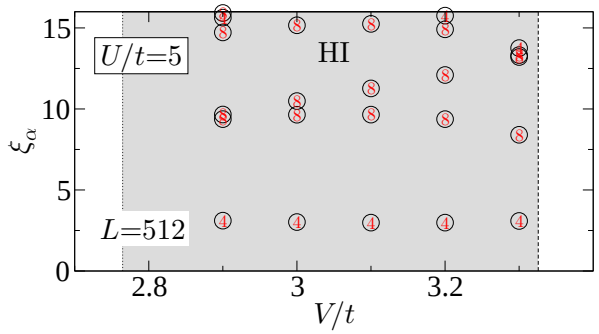

FIG. S2. Entanglement spectrum ξ_α obtained by DMRG in the HI state of the EBHM with $U/t = 5$. The dotted (dashed) line denotes the MI-HI (HI-DW) transition point extracted from the von Neumann entropy, see Fig. 2(a) of the main text. The numbers in the circles give the degree of degeneracy.

Fig. S1 (a), the Mott insulating state and the Haldane state crosses at the MI-HI transition point $V_c(L)$ for the fixed system size used at $U/t = 5$. The transition points obtained for various system sizes can be linearly extrapolated to the thermodynamic limit $L \to \infty$, see Fig. S1(b). We emphasize the perfect agreement with the critical points obtained in the main panel of Fig. 2(a).

Entanglement spectrum in the constrained EBHM

In the HI, due to the broken $\mathbb{Z}_2 \times \mathbb{Z}_2$ symmetry, the lowest entanglement level is four-fold degenerate Since the HI phase is nontrivial protected by the lattice inversion symmetry, not only the lowest but also the entire entanglement spectrum is $4j$-fold degenerate with $j = 1, 2, \ldots$ Figure S2 visualizes the four-fold degeneracy of the higher entanglement levels in the HI phase at $U/t = 5$ for a system with $L = 512$, PBC and $n_b = 2$.

As noticed in the main text, in the weak-coupling regime the central charge $c^*(L)$ strongly depends on the system size [cf. Fig. 2 (c)]. Then the MI-HI (and likewise the SF-HI) phase transition is hard to detect. Figure S3 demonstrates that the situation is similar for the entanglement spectrum calculations at $U = 0$ with $n_b = 2$. Close to the Ising transition point ($U \approx 1.733$) the lowest entanglement level is four-fold degenerate, indicating the existence of the HI phase also at $U = 0$. Increasing the system size the HI state extends to $V \to 0$. Here a more precise finite-size-scaling is desired to pinpoint the MI/SF-HI transition.

Haldane insulator state in the full EBHM

We now demonstrate that the qualitative analysis of EBHM with $n_b = 2$ remains valid if we increase the bo-

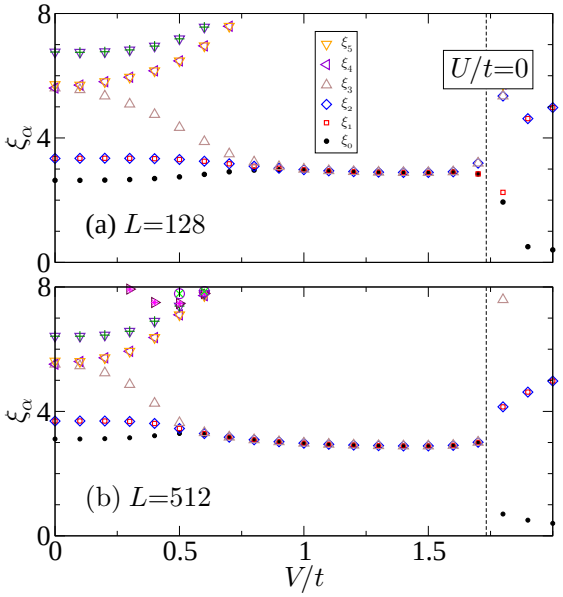

FIG. S3. Entanglement spectrum ξ_α in the weak-coupling (V/t) regime at $U/t = 0$. Data obtained by DMRG with PBCs for $L = 128$ (a) and $L = 512$ (b). The dashed line gives the HI-DW transition point extracted from the von Neumann entropy.

son cutoff. To this end we convinced ourselves that for large enough values of U/t again both MI-HI and HI-DW phase transition points can be determined via the entanglement entropy and the level spectroscopy. For example, at $U = 5t$, the MI-HI phase transition occurs at $V/t \simeq 3.00$ with $c^* \simeq 1.0$ and the system-size dependence of maxima is very weak; see main panel of Fig. S4(a). Adopting level spectroscopy again, the MI-HI transition points can be determined (see inset), yielding excellent agreement with the values in the main panel. The Ising-like HI-DW transition shows up for large system sizes $L > 32$ at $V/t \simeq 3.55$ with $c^* \simeq 0.5$. The entanglement spectrum ξ_α with $n_b = 5$ shows a degeneracy of the lowest level deep in the HI phase for $L = 128$ as in Fig. S4(b). With increasing system size the degenerate HI state extends to the point of the MI-HI transition [Fig. S4(c)].

Finally we show that characteristic behavior of the dynamical charge structure factor $S(k, \omega)$ in the HI phase survives the inclusion of higher boson occupation numbers. Figure S5 presents dynamical DMRG results for $S(k, \omega)$ with $n_b = 5$ deep in the HI phase (for $U/t = 5$, $V/t = 3.3$, $L = 32$ and broadening $\eta = t$). Just as for the constrained EBHM with $n_b = 2$, most of the spectral weights in $S(k, \omega)$ is concentrated around $k = \pi$ and $\omega \ll U$. The maxima of $S(k, \omega)$ follow—as a function of the momentum—the sinus-like dispersion known from the dynamical spin structure factor in the quantum spin-1 Heisenberg model. Note that the system-size dependence of the dispersion in $S(k, \omega)$ is hardly seen in Fig. 4. We conclude that our results for the dynamical structure factor in the HI phase of the constrained EBHM hold qualitatively in the full EBHM as well.

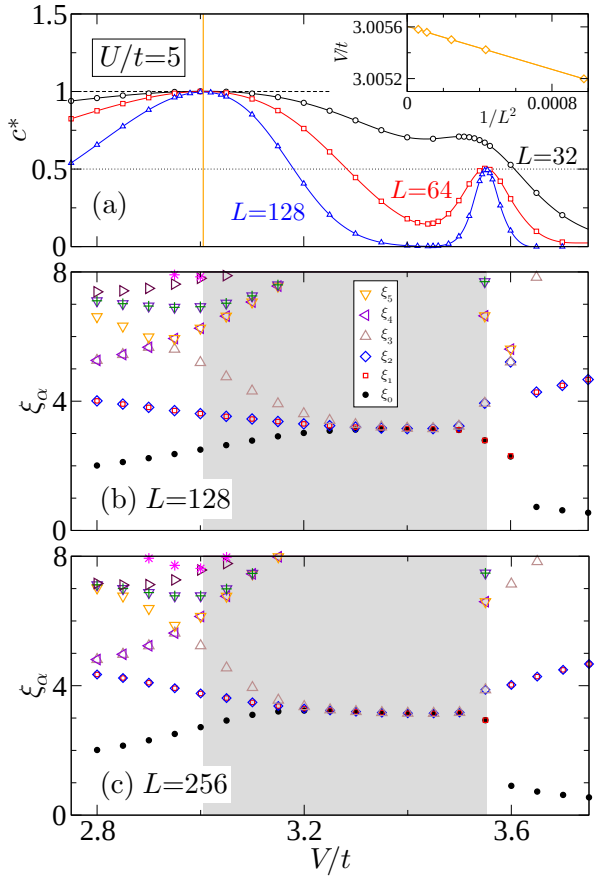

FIG. S4. (a) Central charge $c^*(L)$ at $U/t = 5$ with $n_b = 5$, indicating the MI-HI (HI-DW) transition points with $c = 1$ ($c = 1/2$). ξ_α in the 1D EBHM with $U/t = 5$ for $n_b = 5$ and $L = 128$ (b) respectively $L = 256$ (c).

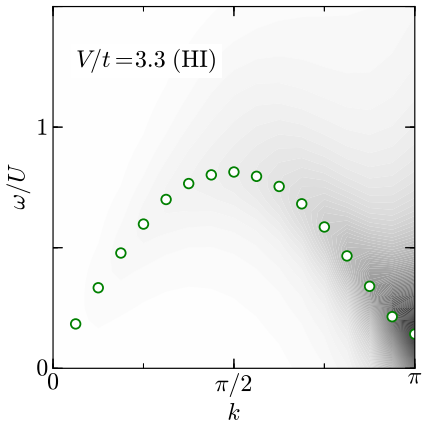

FIG. S5. Intensity plot of $S(k, \omega)$ in the EBHM with cutoff $n_b = 5$. Results were obtained for a lattice with $L = 32$ sites and PBCs, where $U/t = 5$ and $V/t = 3.3$. Within the dynamical DMRG a broadening $\eta/t = 1$ is used. Circles give the maxima in $S(k, \omega)$ for $k = 2\pi j/L$ where $j = 1, \cdots, L/2$.